

CUSTOM DESIGNED ACOUSTIC PULSES

Don C. Lamb,^{†,‡} Jerri Tribble,[†] Apostolos G. Doukas,[‡] Thomas J. Flotte,[‡]
Robert H. Ossoff,[†] and Lou Reinisch[†]

[†]Vanderbilt University Medical Center, Department of Otolaryngology, Nashville, Tennessee

37232-2559; [‡]Wellman Laboratories of Photomedicine, Massachusetts General Hospital,

Department of Dermatology, Harvard Medical School, Boston, Massachusetts 02114

(Paper JBO-199 received Apr. 22, 1998; revised manuscript received Aug. 19, 1998; accepted for publication Sep. 18, 1998.)

ABSTRACT

We have used a tunable, infrared, free-electron laser with a Pockels cell controlled pulse duration to generate photoacoustic pulses with separate variable rise times (from 15 to 100 ns), durations (100–400 ns), and amplitudes (0.005–0.1 MPa). The tunability of the free-electron laser across water absorption bands allows the rise time of the thermal-elastically generated acoustical pulse to be varied, while a Pockels cell controls the duration and cross polarizers control the pressure amplitude. The mechanical effects of pressure transients on biological tissue can have dramatic consequences. In addition to cell necrosis, carefully controlled pressure transients can also be used for therapeutic applications, such as drug delivery and gene therapy. This technique permits systemic probing of how biological tissue is affected by stress transients. © 1999 Society of Photo-Optical Instrumentation Engineers. [S1083-3668(99)00302-0]

Keywords photoacoustic liquids; free electron lasers; biological acoustics; stress waves; computer simulations.

1 INTRODUCTION

It is desirable to understand the biological effects of the laser-induced pressure transients. There are many mechanisms that produce laser-induced pressure transients: optical breakdown, ablation, thermal expansion, electrostriction, and radiation pressure. These mechanisms are extensively reviewed in the literature (see, for example, Ref. 1). The dominant mechanism for acoustic wave generation at lower fluences is thermal expansion. Thermoelastic stress waves are produced by the thermal expansion of the sample after absorption of the laser energy. The exact form of the thermoelastic wave depends on the geometry of the source and sample, the laser temporal and spatial profiles, and the thermal and acoustic properties of the sample. For a more extensive description of thermoelastic stress waves see, for example, Ref. 2.

Recently it has been discovered that pressure waves transiently open the cell membrane, temporarily increasing the permeability of the cell membrane.^{3–6} This effect can be used to enhance the intracellular concentration of different drugs or allow the delivery of drugs that are normally impermeable to the cell membrane while maintaining cell viability.⁷ Larger amplitude stress waves can kill cells directly. Several measurements have shown that shock waves can suppress tumor growth.⁸ Experiments by Doukas et al.⁹ have shown that cell survival decreases with increasing pressure but is also dependent upon the rise time of the pressure

transient. When the fraction of cells that survived was plotted versus the stress gradient (peak pressure divided by the rise time), the data collected at different rise times coalesced, implying that the stress gradient is biologically important. There are indications that the increase in permeability of the cell membrane is also sensitive to the stress gradient (unpublished data).

Although progress has been made in understanding the interaction of pressure transients with tissue, the complete biological effects of pressure transients are not completely understood. One of the main hindrances to the investigation of the biological effects of stress transients has been the inability to control the shape of the stress pulse. In this article, we present a method of controlling the acoustic pulse shape by using the thermoelastic mechanism and pulses from a free-electron laser (FEL).

2 METHOD

2.1 THEORY

For the current discussion we will consider stress waves generated in a fluid, although the one-dimensional solution of the wave equation would be the same for tissue. Provided the rate of thermal expansion is small compared to the speed of sound, the linearized hydrodynamic equations for a homogeneous fluid can be used. If the influence of heat conduction within the sample is negligible on the time scale of the measurements, and nonlinear ef-

Address all correspondence to Lou Reinisch. Tel: (615) 322-7267; Fax: (615) 343-7604; E-mail: reinisl@ctrvax.vanderbilt.edu

fects and attenuation can be ignored, the following inhomogeneous wave equation can be derived:¹⁰

$$\nabla^2 P(\mathbf{r}, t) - (1/c_S^2) \partial^2 P(\mathbf{r}, t) / \partial t^2 = -(\beta / C_p) \partial Q / \partial t, \quad (1)$$

where P is the pressure, c_S is the sound velocity, β is the coefficient of thermal expansion, C_p is the specific heat at constant pressure, and Q is the heat generated from the absorbed laser light per unit volume per unit time. For the experiments reported here, the beam diameter, d , is much greater than the absorption depth of the sample, μ_a^{-1} . Under these conditions, the boundary between the near field (planar waves) and far field (spherical waves) zones, z_f , is given by¹¹

$$z_f = d^2 / 4\lambda_{ac}, \quad (2)$$

where the acoustic wavelength (λ_{ac}) is determined by the absorption depth or the laser pulse duration and the speed of sound depending on whether the absorption depth is greater than or less than the distance of acoustic propagation during the laser pulse. Our sample thickness was always shorter than z_f , allowing the generated acoustic pulses to be treated as planar. The general one-dimensional solution to Eq. (1) for $d/2 > \mu_a^{-1}$ is given by Burmistrova et al.¹² For the work presented here, a rigid boundary was applied to create a unipolar pulse. For a rigid boundary and a spatially uniform laser beam profile,

$$P(\tau) = \left[\frac{\beta I_0}{\mu_a C_p t_L} \right] \left[\frac{1}{2\pi} \right] \int_{-\infty}^{\infty} f(t') K_r(\tau - t') dt', \quad (3)$$

where

$$K_r(\tau - t') = (\pi A^2 / t_L) \exp(-A|\tau - t'| / t_L) \quad (4)$$

is the transfer function of the thermo-optical conversion layer, $\tau = t - z/c_S$ is the reduced time, t_L is the laser pulse width, $A = \mu_a c_S t_L$, I_0 is the laser peak irradiance, and $f(t)$ is the temporal pulse shape. Although the above equation was derived for a spatially uniform laser beam, the same result is obtained for a Gaussian beam profile (TEM₀₀ mode).¹³

In the case where the laser pulse is short compared to the time necessary for an acoustic pulse to propagate a distance equal to the absorption depth, $1/(\mu_a c_S)$, the resulting pressure wave becomes independent of the laser pulse shape. At distances much larger than the absorption depth ($z \gg \mu_a^{-1}$), the pressure is given by

$$P(\tau) = c_S \beta I_0 / (2C_p) \times \begin{cases} [1 - \exp(-\mu_a c_S t_L)] \exp(\mu_a c_S \tau), & \tau < 0, \\ 2 - \exp(-\mu_a c_S \tau) - \exp[\mu_a c_S (\tau - t_L)], & 0 < \tau < t_L, \\ [\exp(\mu_a c_S t_L) - 1] \exp(-\mu_a c_S \tau), & t_L < \tau. \end{cases} \quad (5)$$

In the opposite regime, where the laser pulse is long compared to $(\mu_a c_S)^{-1}$, $A \gg 1$ and $K_r(\tau - t')$ approximates a delta function multiplied by a factor of $2\pi A$. Thus, the acoustic pulse shape follows the profile of the laser pulse,

$$P(\tau) = (c_S \beta I_0 / C_p) f(\tau). \quad (6)$$

The pulse structure of the Vanderbilt University FEL consists of a 5 μ s macropulse composed of subpicosecond micropulses spaced 350 ps apart. The duration of the micropulse ($\ll 1$ ps) is negligible on acoustic time scales. Provided the absorbed energy is rapidly converted into heat, the pressure transient produced by a single micropulse is given by Eq. (5). Since $t_L \ll (\mu_a c_S)^{-1}$, we can approximate the pressure profile at depths $z > \mu_a^{-1}$ as

$$P_\mu(z, t) = P_0 \exp[-\mu_a |z - c_S t|], \quad (7)$$

where P_0 , the peak pressure, is given by

$$P_0 = \mu_a c_S^2 \beta I_0 t_L / (2C_v). \quad (8)$$

From Eqs. (7) and (8) it can be seen that the acoustic wave form generated by a micropulse depends upon the optical absorption coefficient and the sound velocity. Since the peak pressure depends on the absorption coefficient, both the rise time and the amplitude will change with laser wavelength. However, the rise time is independent of laser irradiance so any change in the peak pressure that occurs from varying the laser wavelength can be compensated for by changing the laser irradiance. The amplitude of the acoustic pulse also depends upon the coefficient of thermal expansion and the heat capacity. We use the heat capacity at constant volume, C_v , with the short laser pulses. These parameters are temperature dependent and the shape and amplitude of the acoustic pulses may change as the optical pulse heats the sample. Provided these temperature dependent changes are small, the pressure wave generated by the overall optical pulse can be approximated by a superposition of the pressure transients generated by the individual micropulses:

$$P_M(z, t) = \sum_{i=1}^N I_i P_\mu(z, t - (i-1)t_m), \quad (9)$$

or

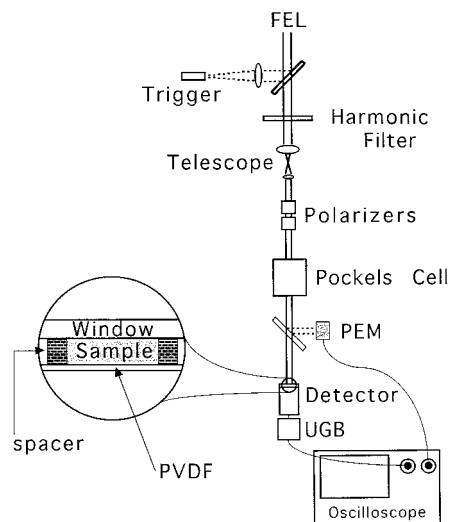


Fig. 1 Schematic diagram of the experimental setup. A small portion of the FEL beam is deflected to a trigger for the Pockels cell. The remaining beam goes through a harmonic filter, a telescope, polarizers, and the Pockels cell before impinging on the sample. The sample path length was either 0.8 or 1.6 mm. A PEM is used to measure the optical pulse after the Pockels cell. The sample is mounted between a sapphire window and the PVDF piezoelectric detector and the output is recorded on a Tektronix transient digitizer. To isolate the detector from the input impedance of the scope, a unity gain buffer (UGB) was used.

$$P_M(z, t) = \sum_{i=1}^N I_i P_0 \exp(-\mu_a(\lambda) |z - c_s[t - (i-1)t_m]|), \quad (10)$$

where I_i is the irradiance of the i th micropulse relative to the peak irradiance I_0 , t_m is the time between micropulses, and N is the number of micropulses in the optical pulse.

2.2 EXPERIMENT

Experiments were performed using the Vanderbilt FEL with a modified output coupler. To control the optical pulse duration, a Pockels cell was designed with a 15 ns rise time and an adjustable duration between 100 and 1000 ns. The timing of the pulse (truncated with the Pockels cell) relative to the leading edge of the macropulse was adjustable, allowing the transmitted region of the macropulse to be selected. A schematic of the experimental setup is shown in Figure 1. The TEM₀₀ output of the FEL was put through an antireflection coated silicon or germanium window to remove the harmonics that would either pass through the Pockels cell or potentially damage the cadmium telluride (CdTe) crystal. The FEL beam was reduced to 3 mm in diameter with a BaF₂ lens telescope and passed through two zinc selenide (ZnSe) Brewster plate polarizers that were used to adjust the laser irradiance. The beam was then passed through a CdTe Pockels cell and an additional ZnSe Brewster plate polarizer. The Pockels cell described by Becker

et al.¹⁴ was used for collecting data at 6.6 μm (EOM3-UC-0347-C-BC, II–IV). All other data were collected with a new Pockels cell (EOM5-2.0-5.0-0540-C, II–IV) which had the following modifications: (1) the crystal faces were perpendicular to the laser beam rather than cut at a Brewster angle and coated with a broad band antireflection coating, and (2) the electronics were reversed so that the laser beam was transmitted only when the high voltage was applied. The extinction ratio of the Pockels cell was at least 150:1. The pulse duration was measured by reflecting a small portion of the laser beam with a BaF₂ window to a photoelectromagnetic (PEM) diode (PEM-L, BSA Technology). The signal was recorded without amplification by a digital storage scope (HP54522A, Hewlett Packard). The sample was mounted on a 9 μm thick polyvinylidene fluoride (PVDF) piezoelectric detector. The propagation distance from the window to the detector was determined by a spacer. A sapphire window was placed over the sample (water for these experiments) and fastened in place by a top plate to provide a rigid boundary. The PVDF detector was coupled to a Plexiglas base for impedance matching and the output was recorded by a transient digitizer (7912 HB, Tektronix). A unity gain buffer was used to isolate the detector from the input impedance of the digitizer. The beam diameter at the sample was 3 mm.

The acoustic detector was calibrated by applying a well defined ballistic pressure (a metal ball was dropped from measured heights). For the 3 mm beam diameter used in our experiments, the sensitivity of the detector was 0.1 bar/mV. The temporal resolution of the transducer and unity gain buffer was tested by measuring the stress wave generated by plasma formation when irradiating aluminum foil with 35 ps pulses from a Nd:YAG laser. The resolution of the system was found to be ~ 6 ns.

All experiments reported here were performed on water. The water was purified by a Milli-Q (Millipore, Bedford, MA) filter system. Absorption from the O–H stretch band of water changes by more than two orders of magnitude between 2.94 and 3.8 μm ,¹⁵ making it possible to produce stress waves with rise times that range from nanoseconds to hundreds of nanoseconds. Experiments were performed at 3.21 μm ($\mu_a = 0.338 \mu\text{m}^{-1}$), 3.30 μm ($\mu_a = 0.140 \mu\text{m}^{-1}$), 3.78 μm ($\mu_a = 0.011 \mu\text{m}^{-1}$), and 6.60 μm ($\mu_a = 0.068 \mu\text{m}^{-1}$). Typical pressures in these experiments ranged from 1/10 to 1 bar. The laser irradiances used for all experiments were believed to be subthreshold for cavitation and other nonlinear effects.

3 RESULTS

Figure 2(a) shows a comparison of single acoustic pulses generated at 3.3 μm with laser pulse durations of 100, 200, 300, and 400 ns at a power of ~ 6 kW during the laser pulse (calculated from 30 mJ of

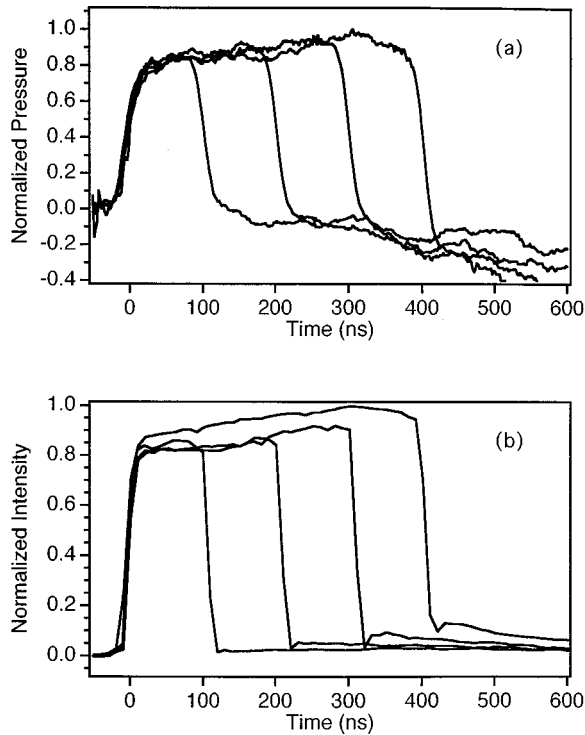


Fig. 2 (a) Acoustic pulses generated with durations of 100, 200, 300, and 400 ns by the FEL at $3.30 \mu\text{m}$. The sample path length was 0.8 mm. The data are displayed as a fraction of the maximum pressure for the entire set (0.14 bar). (b) The corresponding FEL pulses plotted as a fraction of the maximum laser irradiance for the entire set.

energy for a $5 \mu\text{s}$ long pulse). Since we are interested in the pulse shape, the data set was normalized to the maximum pressure of the 400 ns pulses, but the relative amplitudes were unchanged. The corresponding laser profile measured with the PEM diode is shown in Figure 2(b). The rise time and amplitude of the acoustic pulses are independent of duration while the duration of the acoustic pulses follows the duration of the laser pulse. The acoustic pulse begins to form a tensile component with increasing pulse duration. This effect is attributed to diffraction since it increases with acoustic wavelength and sample thickness. We note that the optical pulses show a tail that increases with increasing duration. This phenomenon occurs in the CdTe Pockels cell around $3 \mu\text{m}$ and is dependent on laser irradiance and alignment. However, the optical pulse tail is not responsible for the tensile component of the acoustic pulse since the tensile component is observable in data taken at $6.6 \mu\text{m}$ where the optical tail is absent.

Figure 3 shows single acoustic pulses generated by a 100 ns laser pulse at $3.3 \mu\text{m}$ ($\mu_a c_s t_L = 20.8$) and $3.78 \mu\text{m}$ ($\mu_a c_s t_L = 1.6$) with a pulse power of 6 kW (30 mJ from the $5 \mu\text{s}$ pulse) and 1 kW (5 mJ from the $5 \mu\text{s}$ pulse), respectively. The duration and amplitude of the pulses are similar, but the rise and decay times are markedly different. Experiments were

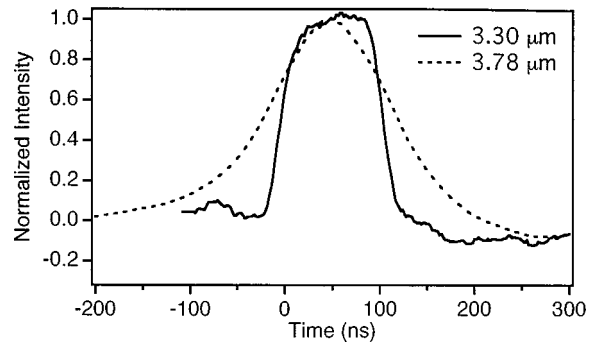


Fig. 3 Acoustic pulses generated by the FEL at $3.3 \mu\text{m}$ (solid line) and $3.78 \mu\text{m}$ (dashed line) with a duration of 100 ns. The sample path lengths were 0.8 mm for the $3.3 \mu\text{m}$ data and 1.6 mm for the $3.78 \mu\text{m}$ data. The data are individually normalized to their maximum pressure (0.14 bar at $3.3 \mu\text{m}$ and 0.45 bar at $3.78 \mu\text{m}$).

performed at $3.21 \mu\text{m}$ with different laser irradiances (Figure 4). The acoustic pulse shape remained unchanged as the laser pulse power was varied from 0.3 to 1 kW (1.7–5 mJ from the $5 \mu\text{s}$ pulse).

Figure 5(a) shows results from experiments at $3.3 \mu\text{m}$ for a 100 ns laser pulse with an average power of 6 kW (30 mJ from the $5 \mu\text{s}$ pulse) measured at depths of 0.8 and 1.6 mm along with the calculated rise time based on Eq. (10). Data and theory for experiments at $3.78 \mu\text{m}$ for a 100 ns, 1 kW average power (5 mJ from $5 \mu\text{s}$ pulse) laser pulse are shown in Figure 5(b).

4 DISCUSSION

The calculated rise time from Eq. (10) using an ideal square pulse for the macropulse envelope is shown in Figure 5(a). The calculated rise time is faster than what is experimentally observed. By using the actual optical pulse to determine I_i in the calculation, the discrepancy was decreased. The remaining difference is most probably caused by the temporal resolution of the detector. The calculations suggest

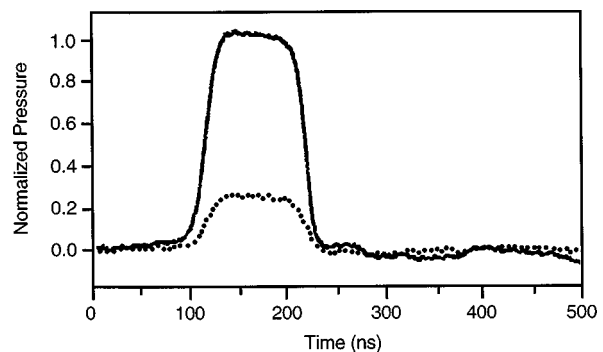


Fig. 4 Acoustic pulses generated at two different laser irradiances by the FEL at $3.21 \mu\text{m}$ with 100 ns duration and a 0.8 mm path length. The stress waves are plotted as a fraction of the maximum pressure at the higher laser irradiance. The maximum pressures were 0.45 bar for the high irradiance pulse and 0.05 bar for the low irradiance pulse.

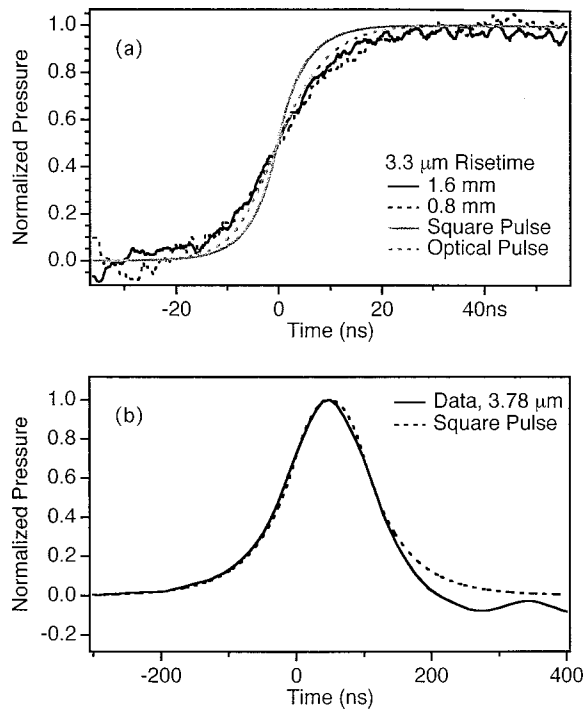


Fig. 5 (a) Rise time of the pressure transient generated by a 100 ns FEL pulse at 3.3 μm observed at depths of 0.8 mm (dark solid line; 0.14 bar actual maximum pressure) and 1.6 mm (dark dashed line; 0.18 bar actual maximum pressure). For comparison, the rise time was calculated using Eq. (10) for an ideal square pulse (gray solid line) and for the actual optical pulse shape (gray dashed line). (b) The experimental (solid line) and theoretical calculation of an ideal square pulse (dashed line) are shown for a stress wave generated by a 100 ns FEL pulse at 3.78 μm (1.6 mm path length). The data and theory are plotted as a fraction of the maximum pressure (actual maximum pressure was 0.45 bar).

that the 10 ns rise time of our optical pulse affects the rise time of the generated acoustic pulse. Using a variable rise and decay time for the optical pulse and the appropriate selection of absorption coefficient, it is possible to experimentally vary the rise time and decay time independently. The Pockels cell electronics can be designed to give a sharp rise time with an adjustable fall time. Then the rise time will be dependent upon the absorption coefficient of the sample while the decay time will follow the envelope of the optical pulse. The reverse scenario is also possible where the rise time depends upon the optical pulse envelope and the decay time is determined by the absorption coefficient of the sample. Thus, all four parameters (rise time, duration, decay time, and amplitude) can be varied independently.

Figure 5(b) shows a comparison between experiment and theory for an acoustic pulse generated by a 100 ns laser pulse at 3.78 μm with 6 kW pulse power (30 mJ from the 5 μs pulse). Here, the acoustic rise time is considerably slower than the rise time of the optical pulse and there is good agreement between experiment and Eq. (10) using an ideal square pulse for the optical pulse envelope.

The data taken at 6.6 μm are similar to the data at 3.78 μm and are not shown here. The results at 6.6 μm signify that the generated acoustic pulse is dependent on the absorption coefficient, but not on the resonance absorbing the laser pulse.

The rise time of the curves in Figure 5(a) shows no significant broadening or steepening and the amplitude shows no significant attenuation between the measured depths of 0.8 and 1.6 mm. Therefore, we feel justified in ignoring the effects of attenuation and nonlinear processes for these measurements. An increase in the tensile component occurs at larger propagation depths, supporting the claim that diffraction is responsible for the formation of the tensile component.

The pulse structure of the FEL is well suited for the generation of custom acoustic pulses. The 350 ps separation of the micropulses delays the onset of nonlinear effects by temporally distributing the laser energy. The micropulses are spaced close enough together that the acoustic pulses from the individual micropulses are not distinguishable. Pressure transients of several hundred ns duration can be created and fit well to the linear superposition of individual acoustic pulses. It is also possible to find a portion of the FEL macropulse that is relatively flat, keeping the laser irradiance constant during creation of the pressure transient.

Figures 2–4 verify that the rise time, duration, and peak amplitude of the generated acoustic pulses can be varied independently. Other methods are available for generating stress waves with variable forms such as laser ablation and the propagation distance through media. Zweig et al.¹⁶ found that the rise times of pressure transients generated by ablating polyamide varied with the laser wavelength. However, they also saw that the rise time changed with the laser irradiance. The dependence of the rise time on the fluence prohibits one from using this method to make a systematic investigation of the biological effects. Allowing the acoustic pulse to propagate through a medium before impinging on the sample can also be used to alter the characteristics of the pressure transient. The attributes of the stress wave depend upon the linear and nonlinear properties of the medium. In general, the sound and particle velocity increases with increasing stress, causing the leading edge of the stress wave to steepen and form a shock wave.¹⁷ The linear acoustic properties of the medium will attenuate the high frequency components of the acoustic pulse. Therefore, the rise time of the stress wave can, in principle, be controlled by choosing the correct propagation distance in a medium with the appropriate acoustic properties. The drawbacks to this approach are that it is cumbersome and the overall amplitude is attenuated.

In the initial studies reported here, the amplitude of the acoustic pulses generated was relatively low. Typical pressures ranged between 1/10 and 1 bar, well below the peak pressures of 0.1–1 kbar cur-

rently used to investigate biological effects. However, the peak pressure can be raised considerably by increasing the laser power, by decreasing the laser spot size, or by using a sample with a larger Grüneisen coefficient. Walsh and Cummings have shown that the optical properties of water change at high laser power.¹⁸ This imposes a limit on what laser irradiances can be used without having to consider nonlinear effects. Vodopyanov measured 100 J/cm^3 as the threshold for photobleaching in water and 100 GW/cm^2 for saturation of the O–H stretching mode as measured with HDO in D_2O .¹⁹ The maximum absorbed energy per unit volume for our experiments was 12 J/cm^3 and the maximum irradiance of the individual micropulses was approximately 30 MW/cm^2 . Nonlinear effects must be considered when using higher irradiance pulses. These nonlinear effects can include the nonlinear response of the tissue to the laser light, the diffraction effects from the nonplanar waves, and the creation of cavitation bubbles. Cavitation was observed for pulse durations longer than 500 ns when the beam diameter was decreased to $\sim 0.5 \text{ mm}$. The peak pressures generated were in excess of 30 bar. Cavitation can be avoided by decreasing the duration of the laser pulse.

The ability to generate short stress waves with fast rise times is an advantage of the thermoelastic mechanism. An acoustic pulse of 10 ns duration in tissue corresponds to a spatial width of $15 \mu\text{m}$. As the spatial rise time and duration decrease, the entire stress pulse will occur over the scale of a single cell and the stress gradient over an even smaller distance. Subnanosecond stress pulses have already been generated in liquids.²⁰ It will be interesting to see what novel effects occur when ultrashort stress waves are applied to tissue. It has been shown that the stress gradient is an important parameter in cellular damage.⁹ With fast Pockels cell electronics, acoustic rise times of 1 ns are achievable. The peak pressure one needs to obtain the same stress gradient decreases as the rise time becomes faster, making it possible to study the biological effects of stress waves using lower peak pressures.

5 CONCLUDING REMARKS

The pressure waves generated by the interaction of lasers and tissue have mainly been considered for the collateral damage that they can cause in biological tissue. However, recently there has been a growing interest in the possible therapeutic applications of these pressure transients. Progress towards clinical applications has been hampered by lack of a detailed understanding of the effects of the characteristic features of pressure transients on tissue. To study these effects, it is necessary to develop methods for controlling the pressure transient parameters independently. In this article we have presented methods for varying the rise time, duration, and peak pressure of the pressure transients. The

rise time is controlled by the absorption depth of the sample that can be varied by changing the wavelength of the laser. The duration is varied using a Pockels cell while leaving the amplitude and rise time unchanged. Cross polarizers alter the pressure amplitude without changing the pulse shape. The macropulse structure of the FEL is ideal for creating custom designed acoustic pulses. The pressures transients generated by the individual micropulses can be summed together to give the shape of the stress wave generated by the whole laser pulse. The 350 ps separation between micropulses extends the pulses durations that one can achieve before nonlinear effects become important. These methods should allow investigators to perform more systematic evaluations of the effects of pressure transients in biological (as well as other) systems.

Acknowledgments

The authors would like to thank Klaus Becker for his help with the Pockels cell electronics. This work was supported by the Department of Defense Medical Free Electron Laser Program under Grant Nos. N00014-87-C-0146 (Vanderbilt University), N00014-91-C-0084, and N00014-94-I-0927 (Wellman Laboratories of Photomedicine).

REFERENCES

1. *Laser Optoacoustics*, V. E. Gusevadn and A. A. Karabutov, Eds., American Institute of Physics, New York (1993).
2. B. Sullivan and A. C. Tam, "Profile of laser-produced acoustic pulse in liquids," *J. Acoust. Soc. Am.* **75**, 437–441 (1984).
3. T. J. Flotte, T. Anderson, D. J. McAuliffe, T. Hasan, and A. G. Doukas, "Laser-induced enhancement of drug cytotoxicity: A new approach to cancer therapy," in *Laser-Tissue Interaction IV*, S. L. Jacques, Ed., *Proc. SPIE* **1882**, 122–129 (1993).
4. S. Lee, T. Anderson, H. Zhang, T. J. Flotte, and A. G. Doukas, "Alteration of cell membrane by stress waves *in vitro*," *Ultrasound Med. Biol.* **22**, 1285–1293 (1996).
5. S. Lee, D. J. McAuliffe, H. Zhang, Z. Xu, J. Taitelbaum, T. J. Flotte, and A. G. Doukas, "Stress-wave-induced membrane permeation of red blood cells is facilitated by aquaporins," *Ultrasound Med. Biol.* **23**, 1089–1094 (1997).
6. D. J. McAuliffe, S. Lee, T. J. Flotte, and A. G. Doukas, "Stress-wave-assisted transport through the plasma membrane *in vitro*," *Lasers Surg. Med.* **20**, 216–222 (1997).
7. S. Gambihler, M. Delius, and J. W. Ellwart, "Transient increase in membrane permeability of L1210 cells upon exposure to lithotripter shock waves *in vitro*," *Naturwissenschaften* **79**, 328–329 (1992).
8. T. M. de Reijke, D. H. Schamhart, K.-H. Kurth, C. W. Löwik, L. H. Donkers, and H. J. Sterenborg, "Tumor growth delay by laser-generated shock waves," *Lasers Surg. Med.* **14**, 205–212 (1994).
9. A. G. Doukas, D. J. McAuliffe, S. Lee, V. Venugopalan, and T. J. Flotte, "Physical factors involved in stress-wave-induced cell injury: The effect of the stress gradient," *Ultrasound Med. Biol.* **21**, 961–967 (1995).
10. P. M. Morse and K. U. Ingard, *Theoretical Acoustics*, p. 324, McGraw-Hill, New York (1966).
11. V. M. Ristic, *Principles of Acoustic Devices*, p. 112, Wiley, New York (1983).
12. L. V. Burmistrova, A. A. Karabutov, A. I. Portnyagin, O. V. Rudenko, and E. B. Cherepetskaya, "Method of transfer

- functions in problems of thermo-optical sound generation," *Sov. Phys. Acoust.* **24**, 369–374 (1978).
13. A. A. Karabutov, A. I. Portnyagin, O. V. Rudenko, and E. B. Cherepetskaya, "Experimental study of the propagation of short thermo-optically excited acoustic pulses," *Sov. Phys. Acoust.* **26**, 162–164 (1980).
 14. K. Becker, J. B. Johnson, and G. Edwards, "Broadband Pockels cell and driver for a Mark III-type free electron laser," *Rev. Sci. Instrum.* **65**, 1496–1501 (1994).
 15. G. M. Hale and M. R. Querry, "Optical constants of water in the 200-nm to 200- μ m wavelength region," *Appl. Opt.* **12**, 555–563 (1973).
 16. A. D. Zweig, V. Venugopalan, and T. F. Deutsch, "Stress generated in polyimide by excimer-laser irradiation," *J. Appl. Phys.* **74**, 4181–4188 (1993).
 17. O. V. Rudenko and S. I. Soluyan, *Foundations of Nonlinear Acoustics*, p. 42, Academic, New York (1977).
 18. J. T. Walsh and J. P. Cummings, "Effect of the dynamic optical properties of water on midinfrared laser ablation," *Lasers Surg. Med.* **15**, 295–305 (1994).
 19. K. L. Vodopyanov, "Saturation studies of H₂O and HDO near 3400 cm⁻¹ using intense picosecond laser pulses," *J. Chem. Phys.* **94**, 5389–5393 (1991).
 20. K. L. Vodopyanov, L. A. Kulevskii, V. G. Mikhalevich, and A. M. Rodin, "Laser-induced generation of subnanosecond sound pulses in liquids," *Sov. Phys. JETP* **64**, 67–70 (1986).